

Growth and characterization of CoTb magnetic thin films

Amalie Terese Jiao Paulsen

amalie.paulsen@etu.sorbonne-universite.fr

Supervisors: Emmanuelle Jal and Marcel Hennes

Number of
pages: 25
figures: 12
characters: 73.130

June 2022

A B S T R A C T

Magnetic thin films consisting of metallic alloys are of particular interest for data recording and spintronic applications. Among them, CoTb is a ferrimagnetic system that can present a perpendicular magnetic anisotropy and distinct periodic magnetic domains with a size of several hundreds of nanometers. The final spin configuration in such thin films is strongly impacted by the alloy composition, thickness and growth condition, but no systematic study has been published so far on these systems. In this report we have grown CoTb thin films with both a buffer layer and a capping layer on Si wafers using magnetron sputtering. We have systematically investigated some key growth parameters in order to optimize the thin film properties. The parameters investigated were: the Si cleaning procedure, the buffer layer, the thickness, the deposition rate, and the alloy composition. The properties of the thin films were characterized primarily using magneto-optical Kerr effect ([MOKE](#)) but also atomic force microscopy ([AFM](#)), energy dispersive x-ray spectroscopy ([EDX](#)), and scanning electron microscopy ([SEM](#)). We found that the best substrate treatment procedure was to use acetone for cleaning before growing a buffer layer of Ta. Then we showed that the alloy composition and the deposition rate greatly influence the magnetic properties. On one hand we evidenced that a change of only 2% of the composition could induce presence or absence of magnetic domains. On the other hand, it seems that a smaller deposition rate yields a better surface quality. However, if chosen too slow, it does not allow to get magnetic domains. A more systematic study of this parameter remains to be performed, in order to further optimize the magnetic structure of these thin films.

CONTENTS

Acronyms	iv
1 INTRODUCTION	1
2 BACKGROUND	2
2.1 A short note on magnetism	2
2.2 Magnetic domains in thin films	4
2.3 Rare earth and transition metal alloys	5
2.4 Goal of the internship	6
2.5 Magnetron sputtering	6
2.6 Characterization	7
2.6.1 Magneto-optical Kerr effekt (MOKE)	7
2.6.2 Atomic force microscopy (AFM) and magnetic force microscopy (MFM)	8
2.6.3 Scanning electron microscopy (SEM) with energy-dispersive X-ray spectroscopy (EDX)	8
3 EXPERIMENTAL SETUP AND RESULTS	9
3.1 Preparing and cleaning the silicon wafers	10
3.2 Magnetron sputtering	10
3.3 MOKE	11
3.4 AFM and MFM	14
3.5 SEM and EDX	15
4 DISCUSSION	16
4.1 The substrate cleaning procedure	16
4.2 Pt or Ta Buffers	16
4.3 The thin film thickness	17
4.4 Deposition rate	18
4.5 Composition	19
5 CONCLUSION	21
Bibliography	23
5.1 Supplementary information SI	25

A C R O N Y M S

AFM Atomic Force Microscopy. [ii](#), [1](#), [7](#), [8](#), [14](#), [15](#), [21](#), [25](#)

CNRS Centre National de la Recherche Scientifique. [1](#)

EDX Energy-Dispersive X-ray spectroscopy. [ii](#), [1](#), [8](#), [13](#), [15–17](#), [19–21](#), [25](#)

INSP Institut des NanoSciences de Paris. [1](#), [14](#), [15](#)

LCPMR Laboratoire de Chimie Physique Matière et Rayonnement. [v](#), [1](#), [10](#), [22](#)

MFM Magnetic Force Microscopy. [8](#), [14](#)

MOKE Magneto-Optical Kerr Effect. [ii](#), [v](#), [1](#), [7](#), [11–13](#), [15–17](#), [21](#), [25](#)

PMA Perpendicular Magnetic Anisotropy. [1](#), [9](#), [11](#), [13](#), [16](#), [19–21](#)

REE Rare Earth Element. [6](#)

SEM Scanning Electron Microscopy. [ii](#), [1](#), [8](#), [15](#), [17](#), [19](#), [21](#)

SI Supplementary Information. [iii](#), [9](#), [12](#), [13](#), [15](#), [16](#), [19](#), [25](#)

TM Transition Metal. [5](#), [6](#)

ACKNOWLEDGEMENTS

A huge appreciation is expressed to my fantastic supervisors: Emmanuelle Jal and Marcel Hennes who have devoted many hours to help me within every area i possible needed it. Further thanks is given to Renaud Delaunay who has designed and build the **MOKE** and magnetron located at the **LCPMR**. Emmanuelle and Marcel have provided invaluable assistance regarding the whole internship and it would not have been the same without their help and good company. I owe them all a huge thanks.

1

INTRODUCTION

The research on magnetic thin films is a rapidly expanding field within both physics and chemistry [1]–[4]. For many technological applications, a complete understanding of the relationship between growth parameters, final structure and magnetic properties is required to achieve the desired functionality. Magnetic thin films consisting of metallic alloys are of particular interest for data recording and spintronic applications [1]. Among them, CoPt (cobalt platinum), a ferromagnetic thin film is widely used [5]. This is because it has distinct repeating magnetic domains with a size of several hundreds of nanometers which are showing maze- or stripe domains depending on how it has been demagnetized [6]. This is partly because CoPt has a strong anisotropy and therefore a difference between the in plane and out of plane magnetization. Due to the lower Curie temperature of CoTb (cobalt terbium), one wants to obtain the same properties using this alloy for thin films. Further, the domain wall dynamics is expected to be much more interesting than for CoPt. However, not enough research has been performed on CoTb thin films in order to state the optimal configuration for repeatable synthesis.

The aim of this project is to systematically optimize the growth conditions of CoTb alloy thin films for obtaining perpendicular magnetic anisotropy PMA and magnetic domains. The goal of this internship is to succeed to control the magnetic properties of CoTb alloy thin films. To do so, we will play with different parameters such as alloy composition, thickness, pressure, cleaning, and buffer layer. The synthesis of the thin films was performed by DC magnetron sputtering and the characterization was performed using MOKE, AFM, EDX, and SEM. The MOKE and the magnetron are located at the Laboratoire de Chimie Physique Matière et Rayonnement (LCPMR) [7]. AFM, EDX, and SEM were done at the Institut des NanoSciences de Paris (INSP).

The Laboratoire de Chimie Physique Matière et Rayonnement (LCPMR) is a mixed research unit between Sorbonne university and the Centre National de la Recherche Scientifique (CNRS). The LCPMR is located at Pierre et Marie Curie campus in Paris, 5e arrondissement. Their primary occupation is within the research field of condensed matter and the interaction between the surfaces of materials and radiation. More specifically the team 'Systèmes fortement corrélés - matériaux magnétiques' uses advanced synchrotron radiation techniques to obtain insight into electron and spin correlation effects and their relationship with the macroscopic properties of complex materials. For that, they need magnetic samples with well defined electronic and magnetic properties that are grown at their laboratory thanks to magnetron sputtering. The Institut des NanoSciences de Paris (INSP) is a joint research unit of CNRS and Sorbonne University with strong expertise in condensed matter physics and nanosciences.

The report is divided into 5 sections: introduction, background, experimental setup and results, discussion and conclusion. In the background section the basics of magnetism and magnetic domains as well as a presentation of the growth and methods of characterization is found. In the experimental setup and results section a review of the data from 19 out of the 33 grown samples is given. The discussion section focuses on five growth parameters: the cleaning procedure, the buffer, the thickness, the deposition rate, and the alloy composition.

2

BACKGROUND

2.1 A SHORT NOTE ON MAGNETISM

It is the electronic configuration of the atoms which determines the magnetic properties in a material. Some electronic configurations will give rise to a magnetic moment in each atom because electrons possess spin- and orbital angular momentum. When a large collection of atoms all have a magnetic moment one can define the vector field, \vec{M} , which is the magnetic moment pr. unit volume [4]. The classification of magnetic materials is determined by their response to an external magnetic field, \vec{H} [8]. **Diamagnetism** is a weak quantum mechanical property found in any material. When a magnetic field is present, the electrons will try to oppose the field by changing their orbital motion which leads to an induced opposite magnetic field [4]. However, it is only the dominant response when all the electrons in the material are paired, as it will induce a zero net magnetic moment. When there is an uneven number of electrons, meaning you have at least one unpaired electron in each atom, a non-zero magnetic moment will arise, leading to stronger interactions. In that case we talk about **paramagnetism**. In these materials, the magnetic moments are aligned randomly in the absence of a magnetic field as seen in fig. 1 A). When a magnetic field is applied, the electrons will align to the magnetic field leading to a momentarily magnetic material [9]. In contrast, in **ferro-, antiferro- and ferrimagnetic** systems, the magnetic moments display ordered configurations in the absence of an external magnetic field as shown in fig. 1 B), C), and D) [8]. These phenomena arise due to unpaired electrons but unlike for paramagnetism, the interaction between spins, called the exchange interaction, is much greater. The **exchange interaction** makes the magnetic moments point in a specific direction. In ferromagnetic materials all the magnetic moments are aligned parallel while for antiferromagnetic materials their alignment is antiparallel [4]. In ferrimagnetic materials, you have some of the magnetic moments parallel and some antiparallel which often occurs in materials containing two or more types of atoms, i.e. alloys. When the two opposite magnetizations do not cancel, there will be a net magnetic moment in one direction. This net magnetic moment depends on the composition of the alloy. The size of the exchange interaction is dependent on the overlap integral between the spins and

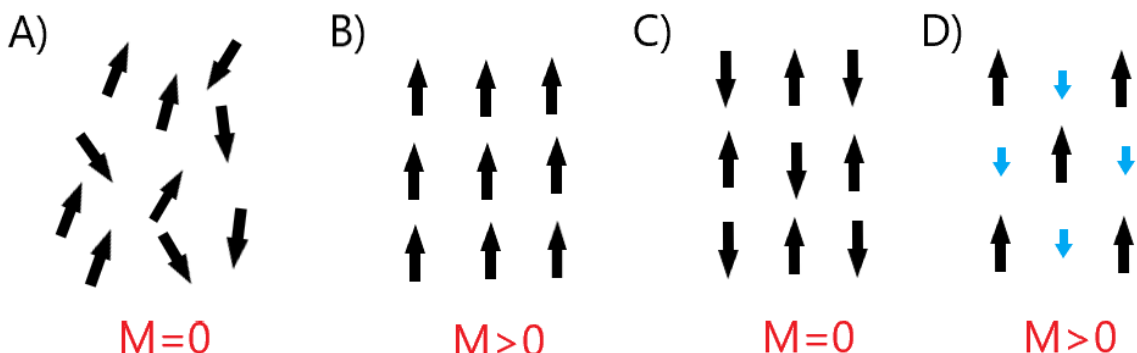


Figure 1: Behavior of magnetic moments in 4 different types of magnetic materials when no external field is applied, $\vec{H} = 0$. A) Paramagnetism, B) ferromagnetism, C) antiferromagnetism, and D) ferrimagnetism.

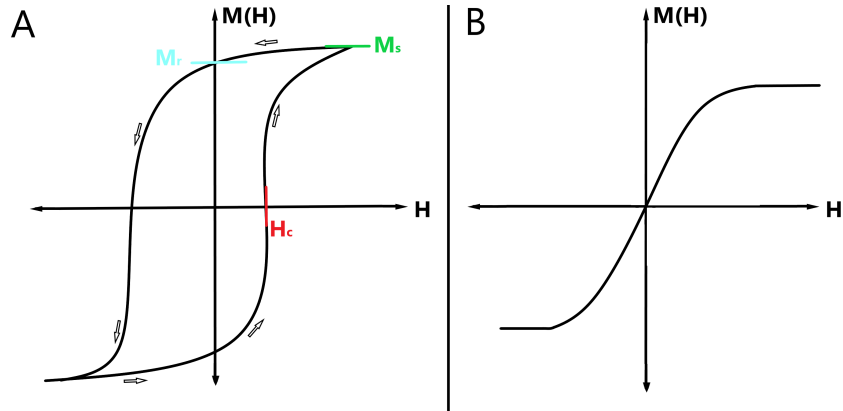


Figure 2: Magnetization curves - Magnetization as a function of external magnetic field. A) Hysteresis for easy axis where M_r is the remanent magnetization, M_s is the saturation value, and H_c is the coercive field. B) Magnetization plotted as a function of external magnetic field for hard axis.

evolves with the temperature. The Curie temperature, T_c is a material dependent constant and is the upper limit for a material to be ferro or ferri-magnetic. Above T_c the material is paramagnetic as the electrons will be excited and therefore have energy enough to overcome the exchange interaction [10]. During my internship I studied only ferri-magnetic materials and will therefore focus on them in the following. Because of their net magnetization, \vec{M} , ferro and ferri-magnetic solids produce their own magnetic field called the **demagnetization field or stray field**, \vec{H}_d . The net magnetization and the demagnetization field points in opposite directions [10] and are able to interact with each other. When an external magnetic field is applied, \vec{H} , the demagnetizing magnetic field, \vec{H}_d , respond by altering the magnetization [4]. The demagnetizing field give rise to **shape anisotropy or magnetostatic energy** which results in some materials having a preferred direction of magnetization and therefore respond differently depending on the orientation of the magnetic field applied. For a uniaxial material, the axis along the net magnetization is called the easy axis while the axis perpendicular to it is called the hard axis [11]. Changing the direction of magnetization between those two axis therefore cost energy and give a measure of this anisotropy, usually defined as the constant K_z . In this project, we are working with magnetic thin films, for which K_z is given by 1 where μ_0 is the vacuum permeability and M_s is the saturation magnetization.

$$K_z = \frac{1}{2} \mu_0 \cdot M_s^2 \quad (1)$$

To characterize a magnetic material, magnetization curves can be measured to know how the system behaves when an external magnetic field is applied in a certain direction. Ferromagnetic materials display hysteresis behavior, where the state of the system depends on its history. Typical magnetization curves for ferro- and ferri-magnets are shown in fig. 2 A) and B). Figure 2 A) is a typical hysteresis curve measured along the easy axis, with H_c being the coercive field found when $M(H) = 0$ and telling you how hard the magnetization of the sample is. Large values of H_c means that the magnet can resist a great external magnetic field without being influenced by it. At $H = 0$ you find M_r which is the remanent magnetization and is a measure of the strength of the magnetization when the magnetic field is absent. M_s is the saturation value which is the upper limit for magnetization of the given material [12]. Fig. 2 B) shows a typical graph where the magnetization is plotted as a function of a magnetic external field applied along the hard axis. The curve is somewhat linear and there is no hysteresis and therefore no coercive field. This is because along the hard axis, the magnetization is proportional to the external magnetic field and therefore near zero in the absence of a magnetic field.

2.2 MAGNETIC DOMAINS IN THIN FILMS

In ferro- and ferri magnetic thin films the magnetic moments point in the same direction. However, looking at the microscopic scale this is not always true throughout the whole surface but only in small areas, called domains. In two domains, the spins are aligned in different directions, called up or down, and are separated by a domain wall [9]. On a large scale, all the domains in a material can cancel each other if there is an equal number of domains pointing in one way as the other. Therefore, it is possible for a ferromagnetic material to have no overall magnetization [4]. The origin of the domains is due to many different interactions at play. The state of the magnetic moments in a material will always be the one which favours the least energetic configuration. In the following, we briefly introduce the different contributions to the magnetic interactions in a metal and how they are minimized.

Exchange interaction: The exchange energy is a short ranged interaction between spins. It originates from the Coulomb interaction and the Pauli exclusion principle and is given by equation 2. Here \mathbf{J} is the overlap integral for the 2 wave functions and J_{ij} is the exchange constant between the two spin moments S_i and S_j of the spins with distance $r_i - r_j$ between them [10].

$$E_{ex} = -J(r_i - r_j) \cdot S_i \cdot S_j \quad (2)$$

For positive values of J , the energy is minimized when the spins are parallel and for negative values of J , the energy is minimized when the spins are anti-parallel. The exchange energy is competing with the excitation of spin magnetic moments. The energy of the excitation is proportional to: $k_B \cdot T$ [10] where k_B is the Boltzmann constant. Above the Curie temperature T_c the energy of the excitation will win over the exchange interaction making the sample paramagnetic as mentioned above.

The **shape anisotropy or magnetostatic energy** describes the interaction between the magnetic moment, \vec{M} and the demagnetizing field, \vec{H}_d , as described above. The minimization of this energy depends on the shape of the sample. For thin films, the energy can be described by eq. 3 where θ is the angle between the surface of the sample and the magnetization and V is the volume [10].

$$E_d = -\frac{1}{2}\mu_0 \cdot M^2 \cdot \sin^2(\theta) \cdot V \quad (3)$$

The **magnetocrystalline interaction** is between magnetic moments, \vec{M} and the electric field produced by the lattice called the crystal field. The crystal field is a potential which the delocalized electrons can feel due to positively charged atomic cores. The magnitude is given by eq. 4 where K_s is the anisotropy constant defined earlier 1 and θ is the angle between the magnetization vector and the axis of easy magnetization [8].

$$E_c = K_s \cdot \sin^2(\theta) \quad (4)$$

The **Zeeman interaction** describes the interaction between the magnetization, \vec{M} and an external magnetic field applied. The size of the Zeeman interaction is given by eq. 5 where \vec{M} is the magnetization of the material and \vec{H} is the external magnetic field applied. The Zeeman interaction is minimized when the magnetization is parallel to the external magnetic field applied [10].

$$E_z = -\mu_0 \cdot \vec{M} \cdot \vec{H} \quad (5)$$

As said previously, the **formation of domains** will mainly arise due to the minimization of all the above contributions. As a consequence of formation of domains: the **domain wall formation energy** can be expressed as in eq. 6. This energy describes the cost to have 2 areas with each their own

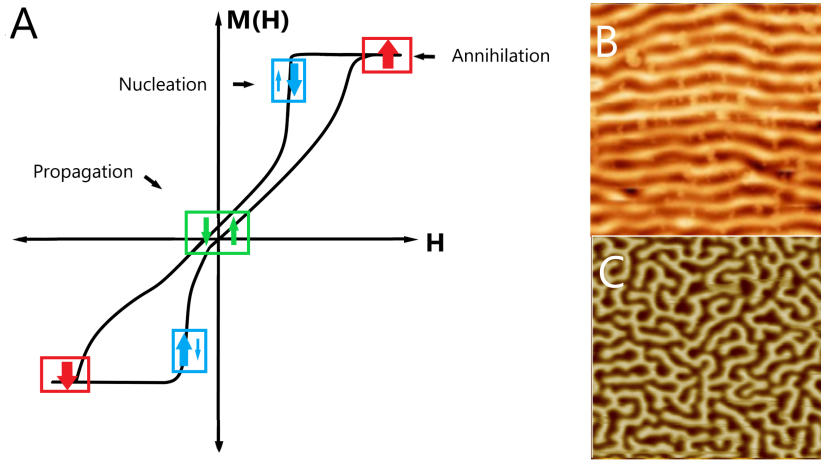


Figure 3: A) Hysteresis of a material with out-of-plane magnetic domains showing the magnetic moments of nucleation, annihilation, and propagation. B) MFM picture of stripe domains taken from [13]. C) MFM picture of maze domain taken from [6].

direction of magnetic moments [4], with K_s being the anisotropy constant and A the exchange constant also called stiffness.

$$E_{DW} = \pi S \sqrt{\frac{2JK_s}{a}} = \pi \sqrt{AK_s} \quad (6)$$

From that we can determine the thickness of the domain wall which is given by eq. 7

$$\delta_{DW} = \pi \sqrt{\frac{A}{K_s}} \quad (7)$$

We see that both the domain wall formation energy and the thickness of the domain wall is dependent on the exchange constant, A , and the anisotropy constant, K_s , which also indicates that the formation and shape of domain walls are highly determined by the short ranged exchange interaction and the long ranged magneto crystalline interaction of the crystal field. Magnetic materials containing domains respond differently to an external magnetic field than materials without domains. This can be seen in the hysteresis of fig. 3. For the description of the typical hysteresis of materials having "up" and "down" domains, one can define three values of the external field: **nucleation field, propagation field, and annihilation field** as seen in fig. 3 A. The nucleation field is the applied field value below which magnetic domains will begin to form. At nucleation field, there is a net magnetic moment in one direction. The propagation field corresponds to the field needed for having a net magnetization of zero because there is an equal amount of domains up and down leading to the cancellation of the net magnetic moment. The annihilation field is the field that needs to be applied to have no more domains. The external field is so strong, that the Zeeman energy overcomes the energies which forms the domains meaning all magnetic moments will point in the direction of the external magnetic field. The most stable domain pattern is a maze, as seen in fig. 3 C) (MFM picture). In the present work, we are interested in aligning the domains into **stripe domains** fig. 3 B) by applying an in-plane field, and then use this alignment as a grating for x-ray experiments [13].

2.3 RARE EARTH AND TRANSITION METAL ALLOYS

Cobalt (Co) is a transition metal (TM) located in the d block in the periodic table. It has delocalized electrons and is a band ferromagnetic material that can be described using the Stoner model. Its magnetic moment at room temperature is typically around $1.7 \mu_B$ (Bohr magneton) [14]. and the Curie temperature is around 1400K [10].

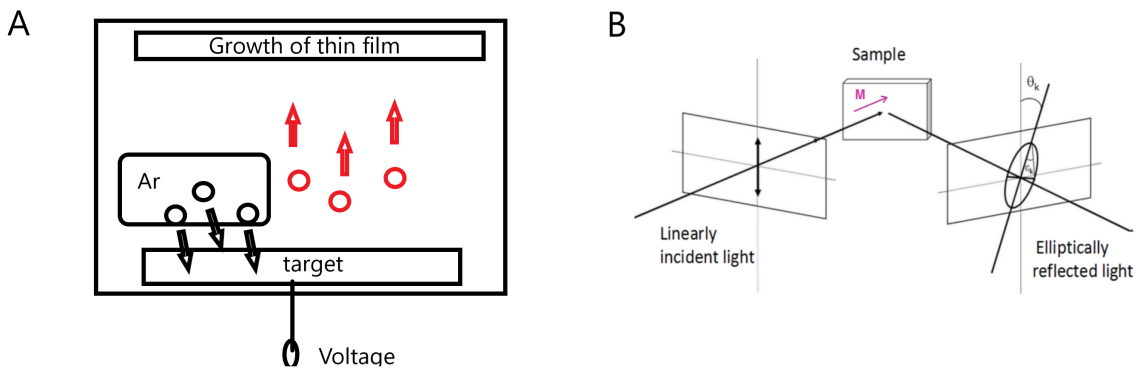


Figure 4: A) sketch of the magnetron principle using Ar as inert gas. B) MOKE principle with linearly incident wave turning elliptical after reflection from thin magnetic film. Taken from [17].

Terbium (Tb) is in the f8 block which makes it a rare earth element (REE). The 4 f electrons are localized on each atom and are therefore not shared amongst the other atoms. Tb has a very high anisotropy which means it has a preferred direction of magnetization, and a high magnetic moment around $9.5 \mu_B$ [15]. However, its Curie temperature is under room temperature (237 K) [10].

When mixing Co and Tb which are a TM and a REE, respectively, interesting magnetic properties arise. This alloy allows to couple Curie temperature above room temperature as well as a high magnetic moment, making it very interesting for devices. Furthermore, their mixing upon sputtering condition creates a strong out of plane anisotropy partially due to the high anisotropy of Tb. Depending on the composition of Co and Tb in CoTb alloy, the magnetic properties will be different [16].

2.4 GOAL OF THE INTERNSHIP

The aim of this project is to find the sample growth conditions to get CoTb thin films with well defined magnetic domains, and eventually perform the type of study that has been done on CoPt [6]. For that we will grow samples thanks to DC magnetron sputtering (next section) and characterize them thanks to MOKE, AFM, SEM and EDX, as I will explain in the next paragraph. The results of this project will allow Emmanuelle Jal and Marcel Hennes to pursue their current study of ultrafast domain wall dynamics [13] thanks to CoTb samples having different magnetic domains (size, orientation, domain wall size). The idea of using CoTb is that due to its lower Curie temperature comparing to CoPt samples, the domain wall dynamics is expected to be much more interesting.

2.5 MAGNETRON SPUTTERING

Magnetron sputtering is a very common technique used for a variety of samples with coatings having electrical or magnetic properties [18]. The technique is very versatile as it is easy to deposit many different kinds of materials at a range of different rates while still obtaining a homogeneous surface throughout the sample. There is further a low occurrence of unwanted events and chemical reactions as the process is carried out using noble non-reacting gasses. The technique allows for thicknesses down to a few nanometer which is of huge importance in thin films as a small change in size can have a great impact on the magnetic properties. The magnetron consists of a vacuum chamber filled with an inert gas. Inside the chamber there are different targets, each connected to a high power supply. A negative voltage is applied to create a plasma thanks to the ionization of the inert gas surrounding

the target. Those ions will hit the target and remove target atoms that will sputter upwards onto the sample as seen in fig. 4 A).

2.6 CHARACTERIZATION

Materials with distinct magnetic properties require a characterization which is sensitive to what kind of magnetism is within the material, how the domains are aligned as well as the magnetic anisotropy that is how the properties are in different directions (geometries). In this project we will use atomic force microscopy (**AFM**) (MFM) which is a good technique for looking at the domains and magneto-optical Kerr effect (**MOKE**) to determine the magnetic anisotropy. Furthermore, because we are working on a sample where the magnetic properties depends strongly on the CoTb alloy composition, we used SEM and EDX to retrieve the exact composition of our samples. Below I will describe the principle of this technique, while the experimental details will be discussed in the next section 3.

2.6.1 Magneto-optical Kerr effekt (**MOKE**)

The magneto-optical Kerr effect (**MOKE**) is one out of many techniques used for studying spin-related phenomena. It is commonly used when investigating magnetic thin films or surfaces as it can give information about the orientation, uniformity and strength of the magnetization down to the mono-layer resolution [17], [19]. The technique is based on the fact that when an electromagnetic waves like light interacts with a magnetic surface, the polarization and intensity is changed [20]. In **MOKE** the polarization rotation of the reflected light beam is directly proportional to the magnetization, \vec{M} , of the material [17]. In order to keep track of the change in polarization, one defines the **scattering plane** also called **the plane of incidence** as the plane containing both the incident and the reflected light beam. There are 3 possible **MOKE** geometries which depend on the direction of the magnetization vector with respect to both the sample plane and the scattering plane: **longitudinal Kerr effect, transverse Kerr effect, and polar Kerr effect**. In the longitudinal Kerr geometry, the magnetization is laying in the sample plane and parallel to the scattering plane. In the polar configuration, the magnetization is perpendicular to the sample plane and parallel to the scattering plane. Lastly, the transverse Kerr effect describes a magnetization which is in the plane of the sample and perpendicular to the scattering plane [17].

The general setup for measuring **MOKE** consists of a laser source with wavelength in the visible to infrared (IR) range which passes through a polarizer which allows you to select a specific polarization and thereby get a known and completely linear polarized beam in either the *s* or *p* direction. *s* and *p* are the abbreviations for *senkrecht* and *parallel* and refers to the direction of the polarization. *s* polarized light has an electric field lying perpendicular to the scattering plane and *p* polarized light has an electric field parallel to the scattering plane making it orthogonal to *s* [17]. We assume that a *s*- polarization is chosen. When the beam is reflected from a metallic and magnetic surface, the polarization can change in 2 ways. The first is the gain of a small *p*-component which leads to a rotation, θ , from its initial polarization. Second, there is a change in the phase between the *s*-polarization and *p*-polarization which leads to an elliptical reflected light whith an ellipticity of, ϵ [17]. The change in Kerr ellipticity and Kerr rotation are very small quantities and therefore, one needs instruments which can measure them with high sensitivity and that we will describe in the next section.

2.6.2 *Atomic force microscopy (AFM) and magnetic force microscopy (MFM)*

The atomic force microscopy (**AFM**) technique is very versatile as it allows one to study the surface of many different types of materials with a high spatial resolution [21]. The **AFM** technique uses the interaction of a small probe with the surface of interest to produce 2D maps of the topography. The general **AFM** setup consists of a flexible cantilever with a nm-sized tip at its end. When the tip is close to a surface, interactions will attract or repel the tip which will result in bending the cantilever. A laser is reflected on this cantilever and the angle of reflection is measured by a quadrant photodiode detector which provides a simple way to monitor the tip - surface interactions. One of the reasons for the versatility is the many modes of the **AFM**. The typical modes for the general **AFM** setup are the contact mode and tapping mode. In the contact mode, the tip is in constant contact with the surface during the scan while in tapping mode the cantilever is oscillating thanks to a piezo. In tapping mode, the cantilever gently "taps" the surface, which modifies the oscillations of the cantilever. A feedback loop is then used to change the vertical position of the latter and adjust the amplitude to a constant setpoint value. The measured z position of the scanning head during a measurement thus gives precise information on the topography of the sample, while keeping tip wear to a minimum. Besides mechanical force, the **AFM** can also use other forces in order to obtain information about electrical, magnetic, chemical, and optical properties [22]. In the electrical modes, a voltage is applied to the cantilever. This mode allows you to look at the conductivity, tunneling current and you can look at how the charges are distributed. In the magnetic mode (magnetic force microscopy (**MFM**)) a magnetic tip is mounted onto the cantilever which can interact with the stray field of a magnetic sample allowing one to see domains [23].

2.6.3 *Scanning electron microscopy (SEM) with energy-dispersive X-ray spectroscopy (EDX)*

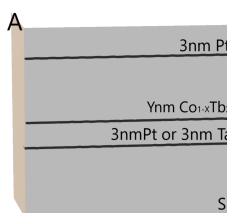
Scanning electron microscopy (**SEM**) and energy-dispersive x-ray spectroscopy (**EDX**) are two techniques which are often used together in order to determine both elemental composition as well as to give a picture with a good resolution of the surface down to a few nanometers. **SEM** is a fast technique to obtain images of the surface structure compared to **AFM** which is much slower due to it's "mechanical" scanning of the surface. However, it does not yield the same information regarding the magnetic properties which is why both techniques are of great importance. **SEM** is a microscope technique using a beam of electrons which interacts with the sample. After interaction, the electrons will be either back scattered or create secondary electrons and they will further emit characteristic X-ray beam depending on the elemental composition [24]. The back scattering and the secondary electrons are used for producing the surface images and can occur in 2 ways namely by inelastic and elastic interactions. In both cases only the electrons bunched back from the surface will be detected and an image with contrast reflecting the topography of the surface will be produced [24]. The **EDX** detector is an extension of the **SEM** and is a precise and fast way to determine the elemental composition and concentration of a sample. The method is based on the fact, that each element has a unique x-ray spectrum. **EDX** is able to detect atoms with more than 5 protons [24] with an accuracy of maximum around 0.5%.

EXPERIMENTAL SETUP AND RESULTS

The aim of this internship was to grow CoTb samples with [PMA](#) and magnetic domains with typical size (periodicity) of several hundreds of nanometers. In order to reach this goal, a systematic study of different growth parameters of CoTb alloys was performed. The CoTb alloys was grown on Si wafers and the general structure of the thin film was: Si/Ta_{3nm} or Pt_{3nm}/(Co_{1-X}Tb_X)_{Ynm}/Pt_{3nm} as seen in fig. 5 A. The different parameters we modified are:

- The cleaning procedure of the Si wafer
- The kind of buffer used (Ta or Pt)
- The thickness Y of Co_{1-X}Tb_X layer
- The deposition rate of the different materials (power of the sources and Ar gas pressure)
- The alloy composition, X = 0.08, 0.10, 0.12, 0.15

A total of 33 different samples were made during this internship. I will however only focus on the 19 samples shown in fig 5. This table summarizes the growth parameters. Column 2 shows the systematic sample names, but for the clarity of this report we will use the numbers in column 1 throughout the report. Column 3 indicates how the Si wafer was cleaned before magnetron sputtering. Column 4 indicates if Pt or Ta was used as a buffer. The composition X of Co_{1-X}Tb_X is shown in column 5 and the grown thickness Y in column 6. Column 7 displays the Ar pressure used during growth (CG1 gauge gives the pressure in 10⁻³mbar), column 8 is the power applied to the Co source in Watt (W), and Column 9 the deposition rate measured in Å/s. All data which are not provided in this report, can be found in supplementary information ([SI](#)).



0	1	2	3	4	5	6	7	8	9
Series nr.	Sample name	Cleaning	Buffer	Composition(X)	Thickness(Y)	pressure Ar	Power Co	Deposition rate	
1		Ta		X=0.12	75nm	2.9*10^-3mbar	60 W	2.1Å/s	
	1.1 20220525_APEJ1	acetone							
2	1.2 20220525_APEJ1	ethanol							
	2.1 20220518_APEJ1	Pt		X=0.12	75nm	12,5*10^-3mbar	90 W	2.2 Å/s	
3	2.2 20220518_APEJ6	Ta							
	3.1 20220523_APEJ1	ethanol	Ta	X=0.12		4.5*10^-3mbar	30 W	1 Å/s	
4	3.2 20220523_APEJ2				20nm				
	3.3 20220523_APEJ3				50nm				
	3.4 20220523_APEJ4				75nm				
	3.5 20220523_APEJ5				100nm				
	3.6 20220523_APEJ6				150nm				
					200nm				
5		acetone	Ta			2.9*10^-3mbar	60 W	2.1Å/s	
	4.1 20220525_APEJ1			X=0.12	75nm				
	4.2 20220525_APEJ2			X= 0.15	75nm				
5	4.3 20220525_APEJ3			X=0.10	75nm				
	5.1 20220531_APEJ1	Acetone	Ta	X=0.1		3*10^-3mbar	60 W	1.9Å/s	
	5.2 20220531_APEJ2				20nm				
	5.3 20220531_APEJ3				50nm				
	5.4 20220531_APEJ4				75nm				
	5.5 20220531_APEJ5				100nm				
5	5.6 20220531_APEJ6				150nm				
					200nm				

Figure 5: A) General detailed layer structure composition of the grown samples. B) Table of the samples mentioned in this report. Column 0 and 1 is the series and number, column 2 the systematic sample name, column 3 the type of cleaning, column 4 the buffer element, column 5 the composition X of Co_{1-X}Tb_X), column 6 the sample thickness, column 7 the Ar pressure, column 8 the power of the Cobalt source, and column 9 the deposition rate. Note that sample 1.1 and 4.1 are the same sample.

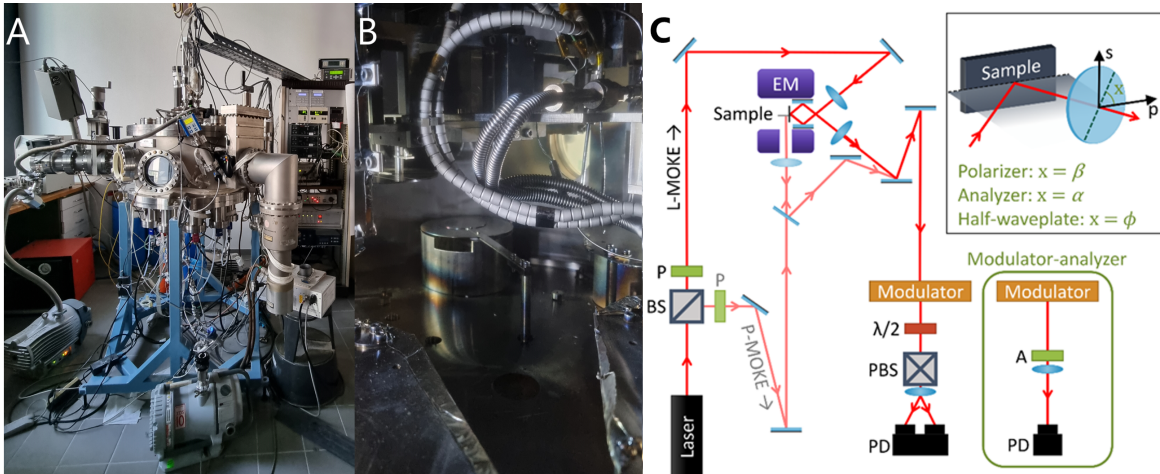


Figure 6: A) Picture of the magnetron setup used in this study. In the middle is the main chamber. The SAS is behind and cannot be spotted. The controls are on the right side. B) Inside the magnetron where the deposition happens. C) Sketch of MOKE setup taken from [25].

3.1 PREPARING AND CLEANING THE SILICON WAFERS

The silicon wafers were bought as three inch buffers precut in squares of $6 \times 6 \text{ mm}^2$ from *Silson company*. To clean the wafers, we tested 2 different initial treatments: cleaning with ethanol and cleaning with acetone. We realized that the different cleaning procedure had an influence on the final magnetic properties (fig. 7 B), even though it is not clear why at the moment. The information one could obtain from this choice was how sensitive the magnetic properties of the thin film was to the dust when grown and how it would influence the repeatability. The cleaning with ethanol and acetone was both performed in a ultrasonic cleaner *Sonoclean* bought from *labo-moderne*. The prepared silicon wafers were stuck with Kapton tape on sample holders specially made for high vacuum environments such as the one of the magnetron interior.

3.2 MAGNETRON SPUTTERING

The samples were grown at the **Laboratoire de Chimie Physique Matière et Rayonnement (LCPMR)** in the magnetron designed and made by Romain Jarrier and Renaud Delaunay seen in fig. 6 A). The LCPMR magnetron uses Argon as the inert gas. The magnetron consists of 2 vacuum chambers; The main chamber where the samples are grown and one with a small volume called the SAS (load chamber). The interior of the main chamber in the magnetron can be seen in fig. 6 B). The SAS and the main chamber are separated by a valve which allows to transfer samples. As said in the previous section, the magnetron sputtering is performed in a vacuum chamber where high vacuum is achieved thanks to a primary and secondary vacuum pump. Due to the small volume of the SAS, it is fast to obtain high vacuum as good as in the main chamber which allows to transfer samples from air to high vacuum easily, without breaking the ultra high vacuum of the main chamber. Every time the valve between the SAS and the main chamber is opened, one has to re-calibrate the parameters of the magnetron before deposition. The magnetron allows for a maximum of 9 samples which can all be grown under the exact same conditions which is a huge advantage when looking at how one parameter influences the growth.

The buffer layer is the first layer deposited on the Si wafer. Si has a very smooth surface and usually a 'binding' layer is grown first before any magnetic layer. In this project Ta or Pt are used. The thickness as well as the composition of the CoTb layer are investigated since in [10], it was shown

that it plays a huge role on the size of the coercive field. The error on the synthesized thickness is unknown for this magnetron but we assume it is systematic. The pressure of Ar as well as the power of the deposited material change the deposition rate that is the rate at which the atoms sputters onto the sample. This rate can change the structural properties of the thin films and therefore its magnetization. The last layer, called the capping layer, prevents the oxidation of the Tb which is very sensitive to oxygen, when the sample is getting out of the chamber to normal atmospheric pressure for magnetic characterization. Therefore, the initial pressure in the main chamber plays an important role when growing samples with Tb as a high vacuum corresponds to low density of oxygen.

3.3 MOKE

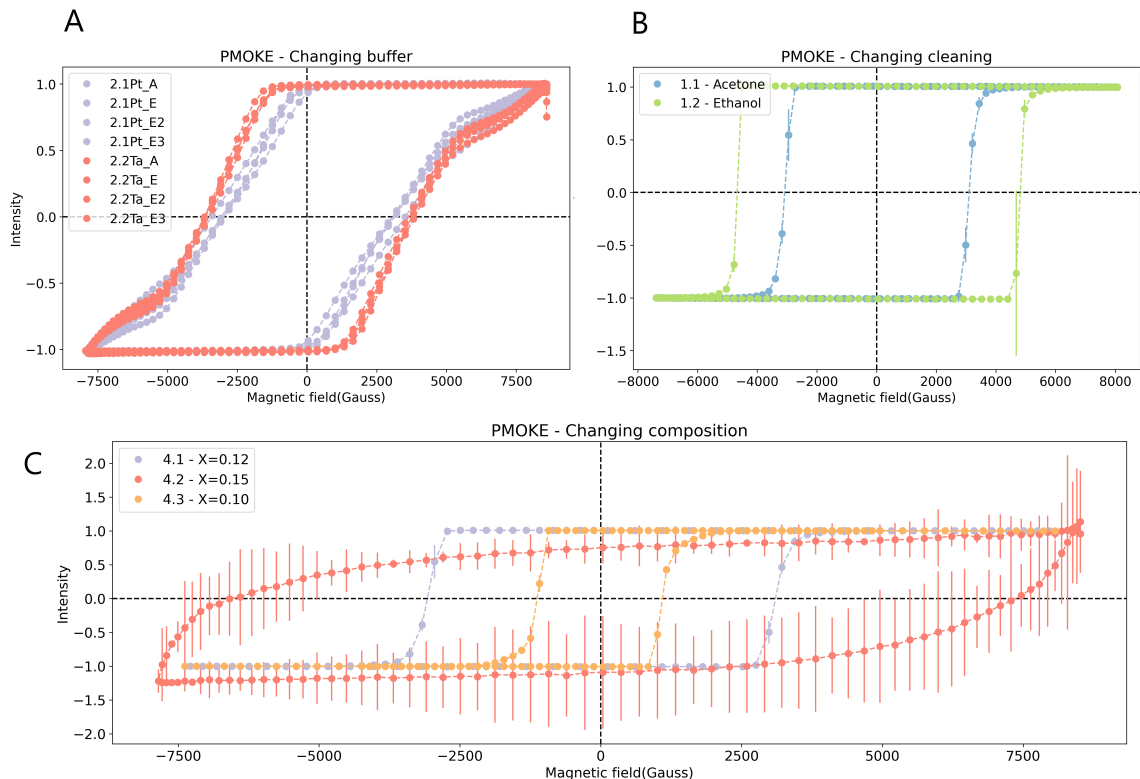


Figure 7: A) PMOKE performed on 4 different spots on 2 samples: 2.1(20220518_APEJ1) where Pt is used as a buffer and 2.2(20220518_APEJ6) where Ta is used as a buffer. B) PMOKE of sample 1.1(20220525_APEJ1) cleaned with acetone and 1.2(20220525_APEJ1) cleaned with ethano. C) Hysteresis of PMOKE of sample series 4 (20220525_APEJ#). Grown under the same conditions but where the composition is changed. 4.1 had a composition of $\text{Co}_{0.88}\text{Tb}_{0.12}$, 4.2 had a composition of $\text{Co}_{0.85}\text{Tb}_{0.15}$ and for 4.3 it was $\text{Co}_{0.90}\text{Tb}_{0.10}$.

MOKE was performed on all the grown samples as the goal of the internship was to find samples with **PMA** and hysteresis similar to the one in fig. 3. The **MOKE** was performed in open air with a HeNe laser (635nm). The laser was sent through a polarizer selecting only the *s* polarization of HeNe. The **MOKE** was carried out using the modulation technique described in Polisetty[19] as seen in fig. 6 C) taken from [25]. The **MOKE** setup consists of a laser which goes through a beamsplitter which allows to use both the setup for polar MOKE (P-MOKE) and longitudinal MOKE (L-MOKE). The mirrors and the focus lenses direct the beam to the sample surface. The magnetic field is applied thanks to an electromagnet which is controlled using a power supply from Kepco. The reflected beam goes through a modulator which sets a frequency to our signal in order to increase the signal to noise ratio thanks to a lock-in detection scheme. To measure either ellipticity or rotation one can choose

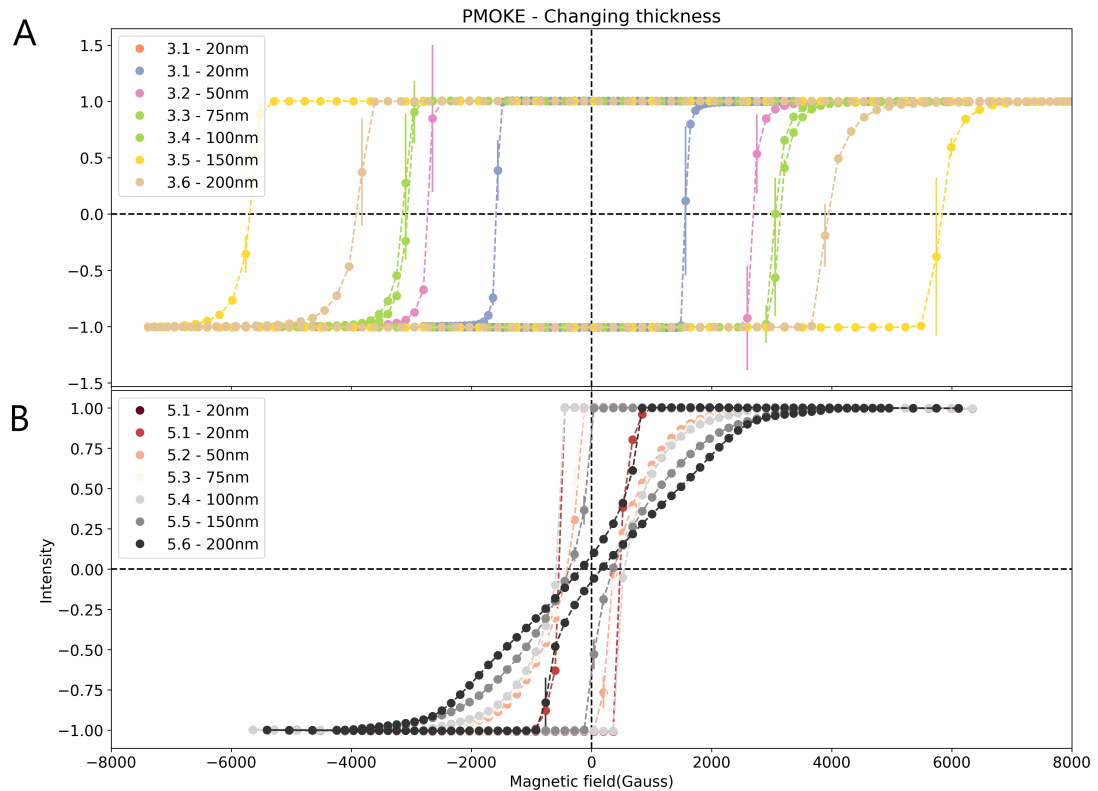


Figure 8: A) Hysteresis of sample series 3(20220523_APEJ#) which is grown under the same conditions but where the thickness is changed. The thickness is ranging from 20nm to 200nm. A total of 6 samples were made in this series. B) Hysteresis showing the final result of the internship of sample series 5 (20220531_APEJ#) grown under the same conditions but where the thickness is varied ranging from 20nm to 200nm. A total of 6 samples were made.

1st or 2nd harmonics on this lock-in detection. The modulator used was from *HINDS* instruments - *PEM 100* controller, and the voltmeter was *Agilent 34401A 6V2* digital multimeter. As mentioned in the previous section, one needs measurements with high sensitivity because the change in the Kerr- ellipticity and rotation is small. Due to this, it is crucial to increase the signal to noise ratio by minimizing the non-magnetic contribution when measuring the Kerr rotation and ellipticity. To detect the modulated signal, we used a lock-in amplifier from *Stanford research systems model SR830DSP* that reads a balanced photodiode from *Thorlabs* which measure the difference in intensity between the *s* and *p* polarization coming out of the wollaston prism (PBS in fig. 6 C). We minimized this signal thanks to a $\lambda/2$ waveplate and to the initial polarizer. Since almost all our samples present an easy axis out of plane, L-MOKE should be linear diagonal for all our thin films. Therefore, we present only the P-MOKE curves and the L-MOKE ones can be found in [SI](#).

All the data from the **MOKE** were extracted and plotted using the python script found in [SI](#). The python script *plot_functions_pmoke.py* contains a function for calculating the standard deviation and mean for an arbitrary number of PMOKE measurements. It thereafter normalizes the intensity to have a value between -1 and 1. Finally, the intensity of the magnetization signal is plotted as a function of the external magnetic field applied (measured in Gauss) where the standard deviation are used as error bars. From these graphs, the information regarding nucleation- and coercive fields are extracted. The **MOKE** data can give a static picture of the change of magnetic properties when changing the different growth parameters.

The first samples were grown based on the parameters of the internship of last year found in SI [26]. We tried to mimic all the same growth parameters: pressure, deposition rate, thickness, and alloy-composition. However, when characterized using MOKE they were surprisingly different from the samples obtained last year found. The first difference is that the buffer layer used was Ta instead of Pt. Usually Ta is used as a buffer layer because it presents a smooth interface. However last year, they was no Ta source available, so Pt was used instead. As this year it was possible to use both we made a comparison between Ta and Pt buffer. Two samples 2.1 and 2.2 were grown under the same conditions but changing the buffer layer from Pt to Ta. The P-MOKE was then measured a couple of times at different spots onto each sample. We found out, that the measurements showed a slightly different hysteresis each time as shown in fig. 7 A). The red curve is the sample with the Ta buffer and the purple curve is the sample with the Pt curve. As the samples with a Ta layer showed a bit less variation in the hysteresis on different spots, the proceeding samples were made with Ta as a buffer.

The second difference between last year and this year is that last year the Si substrate where not cleaned before deposition, while this year because the Si substrate had a lot of dust on them, we washed the Si substrates with alcohol. Therefore we made 2 samples at the exact same time under the exact same condition but where the cleaning of the Si wafers differed. Figure 7 B) shows the cleaning with ethanol (red curve) and with acetone (purple curve). As the acetone showed the hysteresis with the lowest coercive field, the future samples were cleaned with acetone.

From this cleaning and buffer investigation the best MOKE curve is the one of sample 1.1 due to its smaller coercive field (blue curve in fig. 7 B)). However it shows a square hysteresis curve with a rather high coercive field, far from the shape we are looking for (fig 3). To change the coercive field it was shown in [10] that you can play either on the thickness, either on the alloy composition.

In [10] it is shown, that a CoTb composition of $\text{Co}_{0.88}\text{Tb}_{0.12}$ is optimal for creating CoTb alloyos with PMA and stripe domains. We therefore begun by performing a series with different thicknesses for this composition (series 3 of the table 8). The figure 8 A) shows the P-MOKE for thicknesses between 20 nm to 200 nm. These results were very different from the ones found in the literature. Therefore, we then started to change the alloy composition (series 4) as it was shown to have a great influence on the formation of domains.

Figure 7 C) shows the P-MOKE for different alloy compositions of series 4. They are grown under the same conditions but where the composition is changed. 4.1 had a composition of $\text{Co}_{0.88}\text{Tb}_{0.12}$, 4.2 had a composition of $\text{Co}_{0.85}\text{Tb}_{0.15}$ and for 4.3 is was $\text{Co}_{0.90}\text{Tb}_{0.10}$. The error bars on sample 4.2 (red curve) are quite big. This is because the sample is at the verge of having no out of plane anisotropy and a consistent measurement can therefore be a bit difficult to obtain. As neither the cleaning, buffer layer, or thickness of the samples could explain the big differences in the hysteresis we measured the quantitative alloy composition thanks to EDX. This was done in order to see if the theoretical composition stated by the magnetron corresponded with the real one. This is described in the next section. From that investigation it seems the theoretical alloy composition with $X = 0.10$ gives the hysteresis the closest in shape to what we want.

We therefore performed a 5th series for $X = 0.10$ and different thicknesses. As seen in fig. 8 B), we succeed in finding the right parameters for obtaining CoTb magnetic thin films with symmetric nanometer-sized up and down domains (grey and black hysteresis curves). The best samples were sample 5.5 and 5.6 which were analyzed using afm in order to see if the hysteresis shape corresponds well to the presence of distinct magnetic domains.

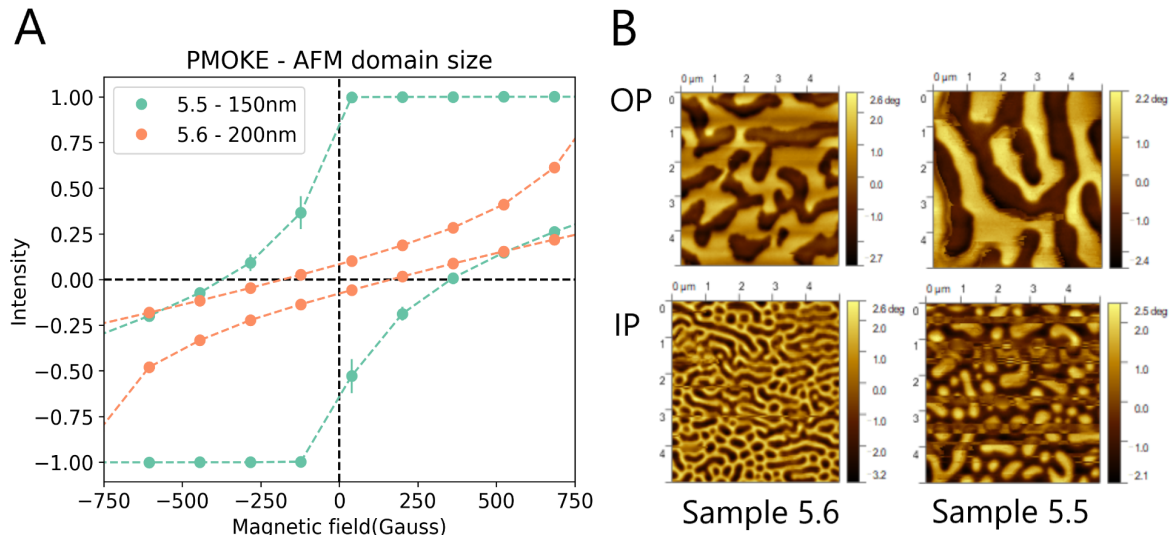


Figure 9: A) Hysteresis zoom on sample 5.5 (20220531_APEJ5) and 5.6 (20220531_APEJ6) B) AFM made on 2 samples: 5.5 (20220531_APEJ5) and 5.6 (20220531_APEJ6) B). OP: is the AFM performed on the samples when they have been magnetized out of plane. IP: is the AFM performed on the samples after they have been magnetized in plane.

3.4 AFM AND MFM

As the goal of this report was to find a CoTb thin film with well defined magnetic domains it was very interesting to look at the samples which showed a hysteresis curve close to the one displayed in fig. 3. The MFM characterization was done at INSP using a Park NX20 AFM [27]. The tips were made of Si and coated with CoCr bought from Bruker and magnetized using a strong permanent magnet. The AFM is placed inside a box which absorbs any vibrations from the surroundings. The characteristic frequency for the magnetic tips are 75 kHz, the lift height was 30 nm. The MFM was performed by scanning the surface 2 times. The first scan is a mechanical scan where the topography is found using the regular AFM technique. The second scan is performed using the magnetized tip. When the magnetized tip is close to a magnetic surface, the stray field of the sample will interact with the magnetic tip on the cantilever. The MFM data is imaging the gradient of the stray field above the sample. The MFM data was analyzed using Gwyddion in order to try to remove the lines and artifacts which were produced by the AFM machine. 4 MFM scans can be found in fig. 9. All the areas investigated were $5\mu\text{m} \times 5\mu\text{m}$ in size and with either 256 or 512 pixels. The corrections made in Gwyddion were the "align rows using various methods", "correct horizontal scars", and "remove polynomial background".

The MFM was performed 2 times on each sample. The first MFM scan was performed after the samples had been magnetized out of plane and the second scan was performed after the samples had been magnetized in plane. This is shown in fig. 9 B). The in plane and out of plane results look very different for both samples. This is common for materials with strong anisotropy. However, we expected that for the in-plane demagnetization, the magnetic domains would have been more aligned than in out-of-plane. But this is not what is observed. It looks quite the opposite. Fig. 9 A) is a zoom on the hysteresis for sample series 5 where sample 5.5 and 5.6 are isolated. The 2 graphs look very different at zero external magnetic field. Sample 5.6 (orange) is very symmetric around zero magnetic field which indicated that there is an equal amount of spin-up and spin down domains. This is different from sample 5.5 (green) which nucleation field slightly favours an un-equal amount of spin-up as spin down domains. We don't understand yet why we do not observe that in the MFM pictures of figure 9.

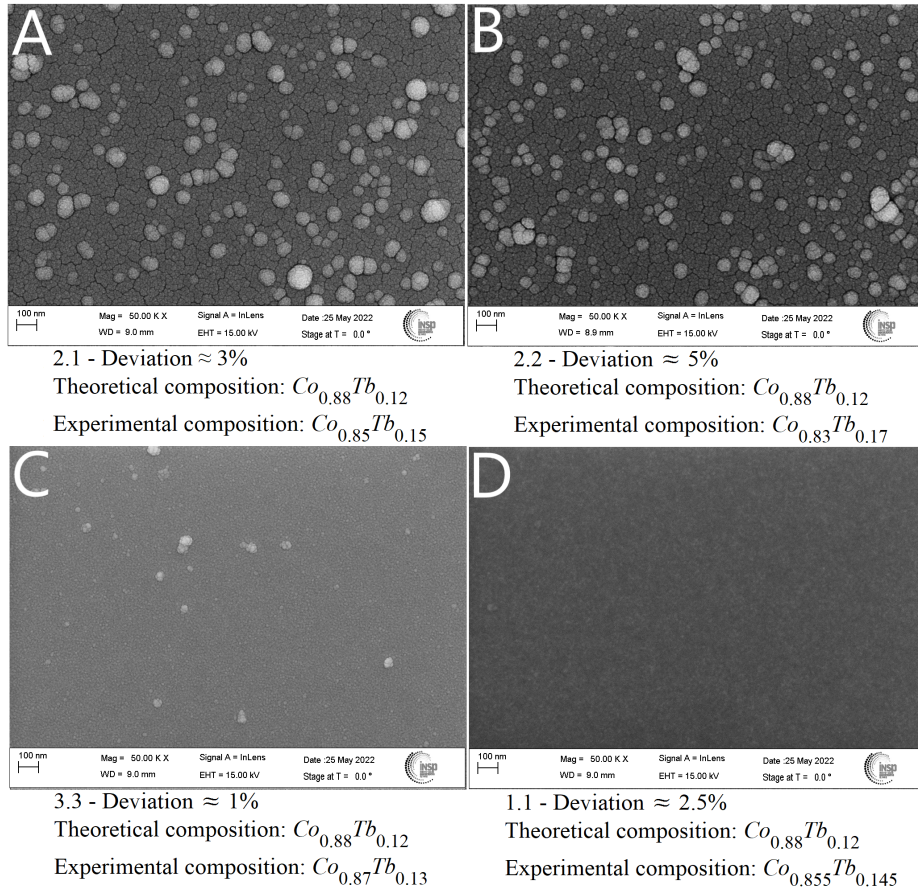


Figure 10: **SEM** and **EDX** showing 4 images of the samples: 2.1(20220518_APEJ1), 2.2(20220518_APEJ1), 3.3(20220523_APEJ3), and 4.1(20220525_APEJ1) found in 5. All the measurements was made of 75nm thin films with a theoretical composition of $Co_{0.88}Tb_{0.12}$. All pictures have a scale of 100 nm.

3.5 SEM AND EDX

As mentioned in the previous section, **SEM** is a very fast and precise technique to image the surface topography. Therefore, this technique was used as it was interesting to know how homogeneous the surface was as well as to know if there were occurrence of big grains or dust as this can have a great impact on the magnetic properties. Further, as the P-MOKE results were not consistent with the ones found in literature it was very interesting to use **EDX** to find the experimental composition as this was not known after magnetron sputtering. The **SEM** and **EDX** measurements were performed at **INSP** using **SEM Zeiss Supra 40** and **EDX Detector** (EDX Compact 30mm Brucker). It was further accomplished under vacuum in a clean room. Due to the high sensitivity, it is very important to minimize the external vibrations and dust. Therefore, the **SEM** was placed on a vibration-cancelling surface. The theoretical occurrence was: C, O, Si, Co, Tb, Ta, and Pt. The energy range which was investigated was from around 0 keV to 11 keV. A total of 8 samples were characterized and they can all be found in the **SI**. A selection of 4 out of the 8 samples investigated are shown in fig. 10 A, B, C, and D. The figure shows the **SEM** and **EDX** of the samples 2.1, 2.2, 3.3 and 4.1 found in fig. 5. All the measurements were performed on 75nm thick samples, all with a theoretical composition of $Co_{0.88}Tb_{0.12}$, and each with a scale bar of 100 nm. We can directly say here that the composition measured is different from the nominal one, and that in the discussion part we will use the real composition. See **SI** for more information on procedure for operation of the magnetron sputtering, the **MOKE**, the **AFM**, the **EDX**, and the **SEM**.

4

DISCUSSION

The goal of obtaining CoTb with [PMA](#) and magnetic domains was met as explained in the previous section. However, the exact impact of the different parameters on the growth and final properties of the samples are still not understood. In the following section an analysis is performed by combining all the results in order to understand how to get well defined domains and repeatability of the samples.

4.1 THE SUBSTRATE CLEANING PROCEDURE

[MOKE](#) was performed on sample 1.1 and 1.2 which were grown under the exact same conditions and at the exact same time but using 2 different methods of cleaning. As seen in fig. 7 B) this resulted in 2 hysteresis with different shape and coercive fields which made it clear, that the cleaning of the sample is important. The difference could be due to the fact that there are some molecules of acetone or ethanol left on the sample at the time of deposition. This could change how the buffer layer binds to the Si wafer which will influence the thin film growth as well as the magnetic properties as seen in the hysteresis.

[EDX](#) was further done on sample 2.1 (A), 2.2(B), 3.3(C), and 4.1(D) as seen in the [EDX](#).fig. 10. sample 2.1, 2.2, 3.3 were all cleaned with ethanol and 4.1 was cleaned with acetone. 2.1, 2.2, 3.3 all show white "bubbles", presumably larger protruding grains, which is a general tendency of the samples cleaned with ethanol and measured in [EDX](#) seen in [SI](#). This was however not investigated systematically and a final conclusion that ethanol is the main reason for the grains cannot be determined. Using acetone for preparing CoTb magnetic thin film samples will however give a smaller coercive field and probably less unwanted structures which is why it should be the preferable cleaning compared to ethanol.

4.2 PT OR TA BUFFERS

The buffer also has an impact on the final magnetic properties since the P-MOKE shows, that there is a difference when growing samples under the same conditions except for the buffer layer purple curves for sample 2.1-Pt buffer and red curves for sample 2.2-Ta buffer in fig 7. Furthermore this Figure 7 shows 4 different hysteresis of sample 2.1 and 2.2 measured on 4 different spots. It is clear, that the hysteresis on both samples changes slightly when changing the spot. Even though this effect is very weak, this is a problem as one of the following factors might change: the thickness of the deposited layer, and/or the CoTb composition are not the same through the sample, and it seems that the type of buffer layer is impacting the growth of the CoTb layer. Even a small contribution from these factors can make a slight change in the magnetic properties on different spots on the sample, and thereby the anisotropy. A further investigation of the anisotropy could have been done by LMOKE measurements on the same spots. Using Ta as a buffer over Pt show that [MOKE](#) measurements on different spots are more alike. This indicates that Ta is probably a better buffer layer compared to Pt,

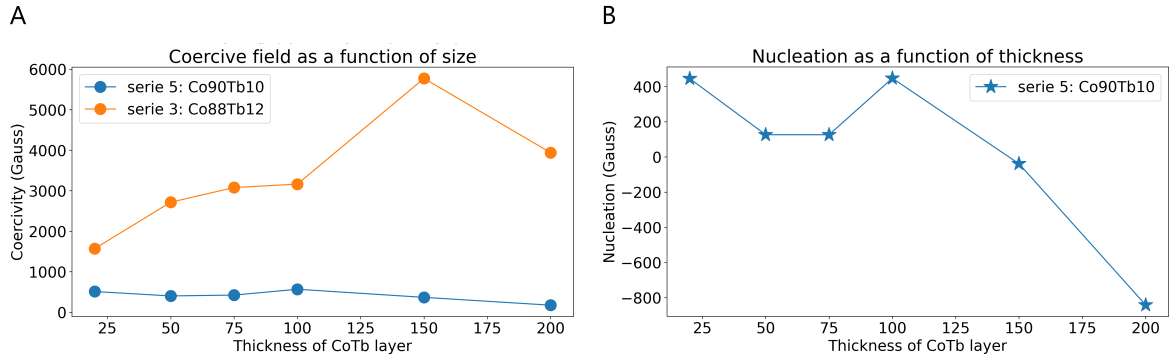


Figure 11: A) Coercive field as a function of size plotted for sample series 5 (20220531_APEJ#)(blue) and sample series 3 (20220523_APEJ#) (orange). B) Nucleation plotted as a function of thickness for sample series 5 ((20220531_APEJ#))

even though, overall, the difference is not huge.

The same samples were measured thanks to [SEM](#) which gave a surface morphology as seen in fig. 10 (A) for sample 2.1-Pt buffer and (B) for sample 2.2-Ta buffer. The [EDX](#) show no immediate difference on the surface topography when one buffer is used over the other. The surfaces are very similar as they both contains big grains. One must conclude, that the buffer does not change the surface structure noticeably.

However we can notice that the composition of the 2 samples was very different. Indeed the measured [EDX](#), show that for the 2 different buffers on samples made the exact same day, there is a very different composition! This is either due to the magnetron sputtering change over the day or to the fact that Pt and Ta bind differently to CoTb. It is currently unknown to us what happened. This could just be coincidental as we already see, that the deviation of the theoretical composition and the experimental composition is quite high compared to the other [EDX](#) measurements of which is only 2,5 and 1 percent off.

Using Ta over Pt as a buffer does not immediately seem to have a huge impact when looking at hysteresis thanks to [MOKE](#) or surface topography thanks to [SEM](#). However, the buffer might change the composition of CoTb found in the [EDX](#). The reason for this is nonetheless still unknown, it might be that the different buffers might interact with the CoTb layer in a different ways.

4.3 THE THIN FILM THICKNESS

Increasing the size of the CoTb layer and leaving all other parameters unchanged, should decrease the coercive field as well as the nucleation field [10]. The coercive field of the different hysteresis of figure 8 are plotted as a function of the thickness. The orange graph is for the third series shown in fig. 8 A) and the blue graph is the fifth series samples shown in fig. 8 B). Both sample series are grown using the same procedure where some initial parameters are chosen and only the thickness of each samples is changed. Both in series 3 and 5, the thickness is ranging from 20nm to 200nm.

We find a bit of a surprising result when looking at the coercive field of sample series 3 (orange). Here the coercive field is increasing as a function of the thickness which is not what we expected as increasing the thickness will normally favor an in plane magnetization implying a decrease of the out of plane coercive field. One must conclude, that not only the thickness plays a role regarding the change in the coercive field. One knows from Gottwald [10] that factors like the composition of CoTb has a lot to say regarding the coercive field. Therefore, we did other series with different

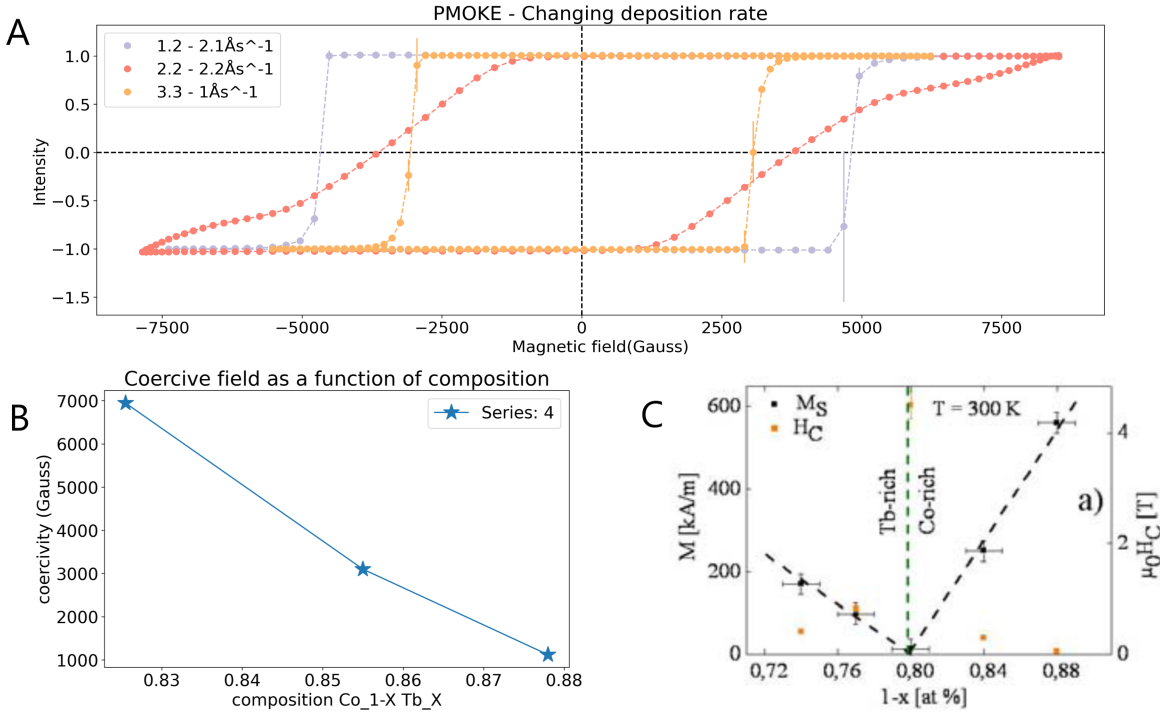


Figure 12: A) 3 PMOKE hysteresis of sample 1.1(20220525_APEJ1), 3.3(20220523_APEJ3) and 5.3(20220531_APEJ3) where the deposition rate was changed. All samples have a thickness of 75nm and were cleaned with ethanol. Sample 1.1 was grown with a deposition rate of 2.1 Å/s, sample 3.3 was grown the a deposition rate of 1. Å/s, and 5.3 with a deposition rate of 1.9Å/s. B) Nucleation plotted as a function of composition of series 4 (20220525_APEJ#) C) Orange dots are the coercive field as a function of composition taken from [10].

alloy composition (series 5). The nucleation field of this series, fig 8 B), is plotted in fig. 11 B). As seen in the fig. 11 A) and B) the coercive- and nucleation field of sample series 5 (blue) decrease with increasing thickness. This is true except for an outlier on fig. B) at 100nm. Currently, it is not known if this is an error when growing the sample or if other factors are at play. In order to explain the increase in the coercive field for sample series 3, one could additionally look at the alloy composition or at the deposition rate. These two factors will be discussed in the following.

4.4 DEPOSITION RATE

The pressure of argon and the power of Co and Tb determines the deposition rate of CoTb. The deposition rate is a measure of how much material is sputtered onto the sample at a given time. This might have an influence on the composition as well as the surface topography and therefore the magnetic properties of our samples.

The sample 1.2, 2.2 and 3.3 are all grown under similar conditions. They are all grown with the same thickness of 75nm, had the same cleaning treatment with ethanol, the same Ta buffer layer, and theoretical composition of $\text{Co}_{0.88}\text{Tb}_{12}$. Sample 1.2 and 2.2 had a deposition rate of 2.1 Å/s and 2.2 Å/s, respectively, which mean the two samples was almost grown under identical conditions. However when looking at the PMOKE in fig. 12 A) one observe that both their coercive field and shape of the hysteresis is very different. Therefore, we will now have look at the Ar pressure and the power of the Co source and not only the deposition rate. It is the power of the Co source and the Ar pressure which together determines the deposition rate. Therefore, one can have 2 very different Ar pressures and Co powers and still obtain the same deposition rate.

Sample 1.2 was grown with a pressure of Ar of $2.9 \cdot 10^{-3}$ mbar and power of cobalt of 60W which gave a deposition rate of 2.2 \AA/s . Sample 2.2 had a Ar pressure of $12.5 \cdot 10^{-3}$ mbar and power of cobalt of 90W which made the deposition rate 2.2 \AA/s . While the deposition rates were almost the same, the power of Co was 1.5 times greater for 2.2 than for 1.2 and the pressure of the Ar 4 times greater. We don't know the exact reason for the tilt of the hysteresis compared to the square but one hypothesis could be that it is due to Ar pressure and Co power too high. To really investigate this problem, one should do a more thorough investigation by growing the thin films where only the Ar pressure and the cobalt power was changed but the deposition rate was kept as well as all other parameters.

Even though one only compare [SEM](#) for sample 1.1 and 2.1 these results seem to indicate that when only looking at the pressure of Ar for the samples, an increase in the pressure is also increasing the size of the grains found. The same tendency is found when looking at the power of Co. This becomes more convincing when looking at the rest of the measurements thanks to [SEM](#) in [SI](#). This seems to indicate a relationship between the grain size of the surface morphology and the pressure of Ar or power of Co.

If we now look at sample 2.2 and 3.3, they are also grown under very similar conditions. Except that the Ar pressure of sample 2.2 as well as the power was 3 times greater than for sample 3.3. When looking at the surface morphology found in [SEM](#) in fig. 10 we see big grains for sample 2.2 while 3.3 is much smoother. Despite a lack of a thorough investigation, our work seems to indicate that the grain size increases with increase in Ar pressure. A more thorough investigation is however necessary in order to confirm this theory.

4.5 COMPOSITION

The samples in series 4 were grown with different composition in order to find the good one to obtain magnetic domains. The figure 12 B) shows the coercive field as a function of CoTb composition X. The hysteresis in series 3 and series 5 look completely different. They are done for the same thicknesses but two different alloy composition and show coercive- and nucleation fields which are very different as seen in fig. 8 and 8 B). What is observed in the [EDX](#) is, that when the deposition rate is small, the theoretical composition should be more close to the experimental one. Indeed, the samples in series 2 were grown with a CoTb deposition rate of 2.2 \AA/s and the [EDX](#) in fig. 10 showed a deviation of around 3 % for sample 2.1 and around 5 %! for sample 2.2 from the theoretical value to the experimental value. The samples in series 1 and 4 was grown with a deposition rate of 2.1 \AA/s which was slightly lower than the one used in series 2 and the [EDX](#) showed a deviation of around 2,5 % for sample 4.1. The samples in series 3 were grown with a deposition rate of only 1 \AA/s . In this case, the [EDX](#) showed a deviation of only 1 % from the theoretical composition to the experimental one. Decreasing the deposition rate made the composition calculated by the magnetron sputtering more reliable to the real one. This makes sense since a lower deposition means a growth which takes longer time which results in the error plays less role in the final composition.

In the series 3, we saw a low deposition rate and an experimental value which was close to the observed one of sample 3.3. However, when plotting all the coercive fields for the different thickness in the series, we saw in the previous section a strange behavior as the coercive field increased with the thickness. This is seen in fig. 11 A). This strange behavior can be due to the fact that a power of cobalt around (30W) implies that the Tb source was only running at 4W which is the lowest used in the whole internship (see [SI](#)). This might have been too low, as we don't know if there was power enough for the Co and Tb to mix in the wanted way. The growth parameters of series 3 resulted in the right composition found in literature for obtaining the [PMA](#) with distinct magnetic domains but as the

power was probably too low, the mixing for obtaining this was not sufficient. It was therefore a delicate balance between a low deposition rate and a high enough power of Co and Tb which resulted in the right PMA and in the formation of distinct magnetic domains. The samples in series 5 were made with an argon pressure around $3 \cdot 10^{-3}$ mbar and power of cobalt around 60W, giving a deposition rate of 1.9 Å/s. Unfortunately, we didn't perform EDX on the series 5 so do not have the real composition values, but if we look at the deposition rate section, one could estimate the composition to be $\text{Co}_{0.90}\text{Tb}_{0.10}$ minus 2 %, leading to a real composition around $\text{Co}_{0.88}\text{Tb}_{0.12}$. This is in good agreement with what is found in [10]. As we can see on the MOKE traces of fig. 8 B) for thick layer (150 nm and 200 nm) we have the same hysteresis shape than in fig. 3. Additionally to having the good composition with the good rate deposition, for this series we also used a different sample holder that allowed to maintain the room temperature during the growth. As the temperature might have an influence on the growth and this was not investigated, one hypothesis is that temperature could also influence the experimental composition vs. the theoretical composition. Making 2 series with the exact same parameters, but where 1 series where the sample is kept at room temperature, and one series where the substrate temperature is not controlled could determine the impact of the temperature on the growth.

Having a low deposition rate will give an experimental composition which are close to the theoretical one. But too low Co power will not give the wanted magnetic properties and too high Ar pressure will probably result in big grains on the surface. Since the deposition rate is determined by the combination of Co power and Ar pressure, one has to play with these three factors in order to obtain the wanted magnetic properties of the CoTb thin film. Our study seems to indicate that a Co power of 60 W with an Ar pressure around $3 \cdot 10^{-3}$ mbar are a good compromise.

CONCLUSION

This project has been a systematic study of the impact of growth parameters on the magnetic properties of CoTb alloy thin films. The aim of the project was to find the parameters to grow magnetic CoTb thin films with perpendicular magnetic anisotropy (**PMA**) and with symmetric stripe domains, ie, equal amount of up and down domains when no external field is applied. The thin films were grown under vacuum using magnetron sputtering where the thickness, pressure of Ar, power of Co and Tb sources, and the cleaning before the sputtering were varied. Afterwards, the magnetic properties were characterized using atomic force microscopy (**AFM**), magneto-optical Kerr effect (**MOKE**), energy-dispersive x-ray spectroscopy (**EDX**), and scanning electron microscopy (**SEM**). We found that growing the samples under the following conditions was the best way to obtain **PMA** and the desired nanometer-sized domains domains of CoTb Alloys.

- Cleaning with acetone instead of ethanol will give a better result as this will result in a smaller coercive field.
- Using Ta as a buffer instead of Pt does not show an immediate difference and is not considered to be the key parameter of getting good **PMA**.
- Changing the thickness will primarily change the coercive- and nucleation field.
- Growing under low pressures (around $3 \cdot 10^{-3}$ mbar) is preferable compared to high pressures (around $12 \cdot 10^{-3}$ mbar) as this will result in a more homogeneous surface without any grains.
- Having a low deposition rate will give a smaller error on the experimental composition. However, there should still be a Co power high enough for getting the wanted magnetic properties.

Thanks to my study, we are close to an optimal and precise configuration of the above parameters for creating CoTb thin film with **PMA** and distinct domains. For the best series made in this internship, the parameters are: washed with acetone, having a Ta buffer, having an Ar pressure of $3 \cdot 10^{-3}$ mbar, a Co power of 60 W, a deposition rate of 1.9 Å/s, and a thickness of either 150nm or 200nm. These parameters gave the wanted hysteresis with **PMA** when measured in **MOKE**. But when measured in the **AFM** the domains were not very distinct and neither out of plane or in plane magnetization gave the wanted result. Therefore, one needs to investigate the growth parameters even more in order to find the optimal configuration. Further investigations could be done on (i) how the cleaning affects the surface morphology, or (ii) a more systematic study of the influence of the deposition rate, or (iii) which influence the temperature has for the alloy composition and mixing, or (iv) trying other alloy composition.

The ability to reproduce the samples is very important for commercial use and it is the goal when growing materials with specific properties. There are still unanswered questions regarding some of the growth parameters which makes the reproducible questionable. Therefore, one needs to gain more knowledge about (i) how the temperature affects the growth and (ii) how the material mixes as this is

crucial for formation of distinct domains. Finally, this study is the starting point of a time resolved characterization in order to give insight on the behavior of the magnetic domains under ultrafast excitation. I am sure that making a more extended investigation of the growth parameters above will allow to gain enough insight not only to make reproducible CoTb alloys sample in the magnetron of the [LCPMR](#) but also in every magnetron.

B I B L I O G R A P H Y

- [1] C. A. F. Vaz, J. A. C. Bland, and G. Lauhoff, “Magnetism in ultrathin film structures,” *Reports on Progress in Physics*, vol. 71, no. 5, p. 056501, May 1, 2008, ISSN: 0034-4885, 1361-6633. DOI: [10.1088/0034-4885/71/5/056501](https://doi.org/10.1088/0034-4885/71/5/056501). [Online]. Available: <https://iopscience.iop.org/article/10.1088/0034-4885/71/5/056501> (visited on 04/26/2022).
- [2] É. du Trémolet de Lacheisserie, Ed., *Magnetism*. Norwell, Mass.: Kluwer Acad. Publ, 2002, ISBN: 978-1-4020-7224-6.
- [3] T. de Lacheisserie, *Magnetism, Materials and Application*. Springer Science + Business Media, Inc., 2005, ISBN: 0-387-23000-9.
- [4] S. Blundell, *Magnetism in Condensed Matter*, 1. publ., repr, ser. Oxford Master Series in Physics Oxford Master Series in Condensed Matter Physics 4. Oxford: Oxford Univ. Press, 2011, 238 pp., ISBN: 978-0-19-850592-1 978-0-19-850591-4.
- [5] O. Hellwig, G. Denbeaux, J. Kortright, and E. E. Fullerton, “X-ray studies of aligned magnetic stripe domains in perpendicular multilayers,” *Physica B: Condensed Matter*, vol. 336, no. 1-2, pp. 136–144, Aug. 2003, ISSN: 09214526. DOI: [10.1016/S0921-4526\(03\)00282-5](https://doi.org/10.1016/S0921-4526(03)00282-5). [Online]. Available: <https://linkinghub.elsevier.com/retrieve/pii/S0921452603002825> (visited on 05/31/2022).
- [6] O. Hellwig, A. Berger, J. B. Kortright, and E. E. Fullerton, “Domain structure and magnetization reversal of antiferromagnetically coupled perpendicular anisotropy films,” *Journal of Magnetism and Magnetic Materials*, vol. 319, no. 1-2, pp. 13–55, Dec. 2007, ISSN: 03048853. DOI: [10.1016/j.jmmm.2007.04.035](https://doi.org/10.1016/j.jmmm.2007.04.035). [Online]. Available: <https://linkinghub.elsevier.com/retrieve/pii/S030488530700649X> (visited on 05/31/2022).
- [7] lcpmr. “Permanent — Physical Chemistry Laboratory - Matter and Radiation.” (2022), [Online]. Available: <https://lcpmr.cnrs.fr/content/permanents> (visited on 05/13/2022).
- [8] C. Kittel, *Introduction to Solid State Physics*, 8th ed. Hoboken, NJ: Wiley, 2005, 680 pp., ISBN: 978-0-471-41526-8.
- [9] D. J. Griffiths, *Introduction to Electrodynamics*, Fourth edition. Boston: Pearson, 2013, 599 pp., ISBN: 978-0-321-85656-2.
- [10] M. Gottwald, “Nouveaux systèmes modèles à aimantation perpendiculaire pour l’étude des effets de transfert de spin,” Sep. 2011.
- [11] M. T. Johnson, P. J. H. Bloemen, F. J. A. den Broeder, and J. J. de Vries, “Magnetic anisotropy in metallic multilayers,” *Reports on Progress in Physics*, vol. 59, no. 11, pp. 1409–1458, Nov. 1, 1996, ISSN: 0034-4885, 1361-6633. DOI: [10.1088/0034-4885/59/11/002](https://doi.org/10.1088/0034-4885/59/11/002). [Online]. Available: <https://iopscience.iop.org/article/10.1088/0034-4885/59/11/002> (visited on 04/26/2022).
- [12] Allenspach. “Course Catalogue - ETH Zurich.” (2022), [Online]. Available: <http://www.vvz.ethz.ch/Vorlesungsverzeichnis/lerneinheit.view?lerneinheitId=158487&semkez=2022S&lang=en> (visited on 05/30/2022).

- [13] M. Hennes, A. Merhe, X. Liu, *et al.*, “Laser-induced ultrafast demagnetization and perpendicular magnetic anisotropy reduction in a Co 88 Tb 12 thin film with stripe domains,” *Physical Review B*, vol. 102, no. 17, p. 174437, Nov. 24, 2020, ISSN: 2469-9950, 2469-9969. DOI: [10.1103/PhysRevB.102.174437](https://doi.org/10.1103/PhysRevB.102.174437). [Online]. Available: <https://link.aps.org/doi/10.1103/PhysRevB.102.174437> (visited on 06/01/2022).
- [14] L. M. Sandratskii and J. Kübler, “Local magnetic moments in bcc co,” *Phys. Rev. B*, vol. 47, pp. 5854–5860, 10 Mar. 1993. DOI: [10.1103/PhysRevB.47.5854](https://doi.org/10.1103/PhysRevB.47.5854). [Online]. Available: <https://link.aps.org/doi/10.1103/PhysRevB.47.5854>.
- [15] R. C. O’Handley, *Modern Magnetic Materials: Principles and Applications*. Wiley, 1999, ISBN: 978-0-471-15566-9.
- [16] T. H. Pham, S.-G. Je, P. Vallobra, *et al.*, “Thermal Contribution to the Spin-Orbit Torque in Metallic-Ferrimagnetic Systems,” *Physical Review Applied*, vol. 9, no. 6, p. 064032, Jun. 20, 2018, ISSN: 2331-7019. DOI: [10.1103/PhysRevApplied.9.064032](https://doi.org/10.1103/PhysRevApplied.9.064032). [Online]. Available: <https://link.aps.org/doi/10.1103/PhysRevApplied.9.064032> (visited on 05/31/2022).
- [17] B. Macias, E. Jal, J. Lüning, and B. Vodungbo, “Development of a setup for time resolved MOKE measurements of ultrafast magnetization phenomena Internship Synopsis,” p. 12,
- [18] P. Kelly and R. Arnell, “Magnetron sputtering: A review of recent developments and applications,” *Vacuum*, vol. 56, no. 3, pp. 159–172, Mar. 2000, ISSN: 0042207X. DOI: [10.1016/S0042-207X\(99\)00189-X](https://doi.org/10.1016/S0042-207X(99)00189-X). [Online]. Available: <https://linkinghub.elsevier.com/retrieve/pii/S0042207X9900189X> (visited on 04/26/2022).
- [19] S. Polisetty, J. Scheffler, S. Sahoo, *et al.*, “Optimization of magneto-optical Kerr setup: Analyzing experimental assemblies using Jones matrix formalism,” *Review of Scientific Instruments*, vol. 79, no. 5, p. 055107, May 2008, ISSN: 0034-6748, 1089-7623. DOI: [10.1063/1.2932445](https://doi.org/10.1063/1.2932445). [Online]. Available: [http://aip.scitation.org/doi/10.1063/1.2932445](https://aip.scitation.org/doi/10.1063/1.2932445) (visited on 04/26/2022).
- [20] A. Kirilyuk, A. V. Kimel, and T. Rasing, “Ultrafast optical manipulation of magnetic order,” *Reviews of Modern Physics*, vol. 82, no. 3, pp. 2731–2784, Sep. 22, 2010, ISSN: 0034-6861, 1539-0756. DOI: [10.1103/RevModPhys.82.2731](https://doi.org/10.1103/RevModPhys.82.2731). [Online]. Available: <https://link.aps.org/doi/10.1103/RevModPhys.82.2731> (visited on 04/26/2022).
- [21] H. Sharma and N. Negi, “Structural and Magnetic Investigation of Cu, Co Substituted NiFe₂O₄ Thin Films by Scanning Probe Microscopy (AFM, MFM),” *Materials Science Forum*, vol. 830–831, pp. 589–591, Sep. 2015, ISSN: 1662-9752. DOI: [10.4028/www.scientific.net/MSF.830-831.589](https://doi.org/10.4028/www.scientific.net/MSF.830-831.589). [Online]. Available: <https://www.scientific.net/MSF.830-831.589> (visited on 06/15/2022).
- [22] “What is AFM? Learn about Atomic Force Microscopy! - NanoAndMore.” (), [Online]. Available: <https://www.nanoandmore.com/what-is-atomic-force-microscopy?gclid=Cj0KCQjwhqaVBhCxARIsAHK1tiNNbDzfox5Yxheblyueg6ZTrozENEXUKwCB> (visited on 06/15/2022).
- [23] G. Haugstad, *Atomic Force Microscopy: Understanding Basic Modes and Advanced Applications*, 1. ed. Hoboken, NJ: Wiley, 2012, 464 pp., ISBN: 978-0-470-63882-8.
- [24] M. Abd Mutualib, M. Rahman, M. Othman, A. Ismail, and J. Jaafar, “Scanning Electron Microscopy (SEM) and Energy-Dispersive X-Ray (EDX) Spectroscopy,” in *Membrane Characterization*, Elsevier, 2017, pp. 161–179, ISBN: 978-0-444-63776-5. DOI: [10.1016/B978-0-444-63776-5.00009-7](https://doi.org/10.1016/B978-0-444-63776-5.00009-7). [Online]. Available: <https://linkinghub.elsevier.com/retrieve/pii/B9780444637765000097> (visited on 06/15/2022).

- [25] Légaré, “Analytic description and optimization of magneto-optical Kerr measurements,” 2022.
- [26] C. Vang, “Croissance et caractérisation magnéto-optique de couches minces ferrimagnétiques CoTb,” p. 25, 2021.
- [27] park. “Atomic Force Microscopy Systems — AFM System — Park Systems.” (2022), [Online]. Available: <https://www.parksystems.com/> (visited on 05/13/2022).

5.1 SUPPLEMENTARY INFORMATION SI

https://github.com/zheezit/Internship_2022/ link to repository containing **Supplementary Information (SI)** which includes:

- Bibliography
- Procedure
 - MOKE
 - Magnetron
 - AFM
- Data
 - MOKE
 - AFM
 - EDX
- Python code
 - plot_functions_pmoke.py
 - plot_funxtion.py (both PMOKE and LMOKE)